The Journal of the Astronautical Sciences (2018) 65: 377–399
https://doi.org/10.1007/s40295-018-0136-x

Volume Multi-Sphere-Model Development Using Electric Field Matching

Gabriel Ingram[1] · Joseph Hughes[1] · Trevor Bennett[1] · Christine Reilly[1] · Hanspeter Schaub[1]

Published online: 16 November 2018

Abstract

Electrostatic actuation is the process of charging two spacecraft and using the resulting Coulomb interaction to exert touchless forces and torques between the two spacecraft. For all electrostatic actuation concepts, fast and accurate models for the electrostatic force and torque are needed. The Volume Multi-Sphere Method (VMSM) seeks the optimal placement and radii of a small number of equipotential spheres to accurately model the electrostatic force and torque on a conducting space object. Prior work optimized the VMSM models by varying the radii and position of the model spheres to match the force and torque produced by a finite element truth model. This process is challenging due to finite element model errors and smoothness considerations, as well as because the force solutions are dependent on the particular probe geometry chosen. This paper investigates fitting of VMSM models to Surface-MSM (SMSM) generated electrical field data, removing modeling dependence on probe geometry while significantly increasing performance and speed. A proposed electric field matching cost function is compared to a force and torque cost function. The inclusion of a self-capacitance constraint is explored and 4 degree-of-freedom VMSM models generated using electric field matching are investigated. The resulting E-field based VMSM development framework is illustrated on a box-shaped hub with a single solar panel. Despite the complex non-symmetric spacecraft geometry, elegantly simple 2-sphere VMSM solutions provide force and torque fits within a few percent.

Keywords Electrostatics · Proximity opperations · Orbital debris

✉ Joseph Hughes
joseph.hughes@colorado.edu

[1] Department of Aerospace Engineering Sciences, University of Colorado, Boulder, CO, USA

Introduction

Electrostatic modeling of spacecraft and space debris is currently an active area of research with applications in Space Situational Awareness (SSA), [1, 2] Lorentz Augmented Orbits (LAO) [3] and touchless interaction between spacecraft [4–6]. To simulate any of these dynamical systems, a faster-than-realtime method of computing the electrostatic forces and torques is required to perform any numerical performance and stability analysis. Spacecraft and debris in both Low Earth Orbit (LEO) and Geosynchronous Earth Orbit (GEO) can become charged by interactions with ambient plasma to such an extent that they are perturbed by Earth's electric and magnetic fields [7, 8]. Although accelerations caused directly by Lorentz forces are small in both LEO and GEO, electromagnetic influence on attitude can cause variation in more prominent attitude-dependent perturbations–such as solar radiation pressure–that lead to significant changes in orbital parameters in a matter of hours [1, 8]. Objects that are particularly affected by this phenomenon are those with high area-to-mass ratios, HAMR objects, which constitute part of the debris population [1, 2]. Improvements in satellite propagation and orbit determination of such debris objects requires electrostatic modeling of some form. Computational efficiency is desirable in both trajectory propagation, and orbit determination.

In addition to natural orbit evolutions, when spacecraft or debris charges are controlled artificially using ion or electron beams, both Lorentz and Coulomb forces can be harnessed for useful purposes, such as LAO, active debris removal and touchless de-tumbling of spacecraft [3, 9, 10]. LAO applications are varied, and include drag compensation in elliptical orbits, inclination control, and rendezvous [3]. Lorentz forces can be used to augment formation flying reconfiguration control laws to reduce thruster ΔV requirements, and for limited propellentless propulsion [11–13].

While LAO exploit the Lorentz force experienced by spacecraft moving quickly through a magnetic field, Coulomb forces between spacecraft and debris can also be utilized. Electrostatic tugging is proposed as a means of active debris removal and for applications in formation flying [9, 14, 15]. The Geosynchronous Large Debris Reorbiter (GLiDeR) is one active debris removal concept that harnesses these electrostatic effects. The GLiDeR remotely charges a defunct satellite or piece of space debris with an electron beam, allowing it to interact with the object for the purposes of changing the object's orbit. Orbit raising of 250 km can be accomplished in a little over two months using Coulomb interaction between GLiDeR and a target [6]. Electrostatic de-tumbling of space objects is currently being researched, and shows promise as a method for reducing debris tumbling rates to within an acceptable magnitude for grappling in servicing missions [10, 16–18].

Many of these applications motivate and require faster-than-realtime methods of electrostatic force and torque modeling. Although finite element method (FEM) software, such as ANSYS Maxwell 3D©, provides accurate results, calculations of the force and torque between a target and command spacecraft at one relative position and orientation requires time on the order of minutes. To simulate charged attitude motion in a Geosynchronous orbit with even a coarse one second time step requires a long numerical simulation time approaching a year. The duration of this calculation

is unacceptable for control analysis purposes. The Multi-Sphere Method (MSM) is a lower-fidelity electrostatic modeling technique that can be evaluated quickly enough for faster-than-realtime applications [19, 20].

MSM is an elastance-based method for predicting the force and torque on conductors [21]. It is similar to the method of moments in its linear form, but differs in that the size and location of the nodes are hand-tuned rather than derived from first principles [22]. This tuning is done by an optimizer to match forces and torques which are computed using a high-fidelity FEM software. Because of this, MSM can predict Coulomb forces and torques very quickly at accuracies of 1-2% or better depending on the separation distance of the charged objects. Recent work largely automates the process of generating MSM models using local optimizers; however, challenges to current MSM model generation methodologies remain [7]. In particular, current automation of Volume-MSM (VMSM) modeling is accomplished by fitting to FEM generated force and torque data. Not only is the process of generating FEM data time consuming, but it is prone to producing noisy force and torque data if the objects are far apart. The effect of noisy data is mitigated by fitting to near-field data and imposing a self-capacitance constraint upon the optimization process. The self-capacitance constraint ensures that the total charge on an isolated MSM model with a prescribed voltage is the same as predicted by FEM, and exploits the simplified field behavior of the problem at large radial distances where even complex geometry can be accurately approximated as a point charge. In addition, fitting to force and torque data ties the resulting VMSM model to a specific probe geometry, which lacks generality.

This paper develops a novel automated method of generating VMSM models by matching the electric field in the vicinity of the target rather than Coulomb forces and torques. This has two benefits: 1) The E field data is computed with Surface MSM (SMSM), which is much smoother than FEA data and makes optimization easier, and 2) The E field can be computed without another body (unlike the force and torque), which adds generality. The E-field fitting greatly reduces the time required to generate a VMSM model while maintaining the model accuracy associated with current modeling techniques. Of interest is how well this E-field fitting technique functions on complex shapes that are not simple spheres or cylinders as in the earlier VMSM and SMSM work. As discussed in Reference [7], imposing the spacecraft's self-capacitance constraint can improve the MSM fit quality for large separation distances. This paper explores how imposing the self-capacitance constraint impacts the MSM setup performance.

The paper is structured as follows. A brief review of the Multi-Sphere method is presented. The optimizer cost functions for current VMSM and E-field matching model generation methodologies are compared near a solution. Force and torque model accuracies when the E-field matching method is applied to a complex asymmetric box-and-panel geometry, with and without a self-capacitance constraint, are investigated. The computational effort of producing one, two and three-sphere VMSM models of the box-and-panel geometry is detailed. The effect of data reduction on model accuracy when a self-capacitance constraint is imposed is shown, and a comparison between the accuracies of reduced-coordinate and 4 degree-of-freedom models is made.

Multi-Sphere Method Background

MSM provides a computationally fast approximate model of a spacecraft's electrostatic properties for applications that require faster-than-realtime results. MSM solves for the force and torque on a conductor by first finding the charge on a number of virtual spheres placed within the body. The charge on the spheres is found by assuming all spheres are equipotential across a single space object and solving a linear system of equations. The equipotential voltage of the spacecraft is found with current-balance methods [23] and is assumed to be known perfectly in this analysis. MSM divides into VMSM, which uses a small number of spheres placed within the *volume* of the conductor, and SMSM, which places a large number of spheres on the *surface* of the conductor. It is more difficult to generate VMSM models because the size and location of the spheres must be found using an optimizer; however, VMSM models are much faster to run once completed due to the much smaller number of spheres employed. In contrast, SMSM models are easier to set up because the spheres are placed uniformly on the spacecraft. For rectangular spacecraft this is done using a grid, and for cylindrical and spherical shapes this is done using a golden spiral [24]. Once the positions are found, the sphere size can be found by matching self-capacitance, which is computed from commercial FEM software. Generally, SMSM models show higher accuracy than VMSM models when compared to FEM-generated force and torque data [2]. Although SMSM greatly reduces the effort required to create a MSM model for a given spacecraft geometry and increases the accuracy of the model, it comes at increased computational cost at runtime due to the larger number of spheres.

Both the Volume Multi-Sphere Method and Surface Multi-Sphere Method represent a conducting object as N spheres, as shown in Fig. 1. These methods only differ in the number, size and placement of the spheres used to represent the conductor. The MSM formulation currently assumes that the surface of the target craft or debris is perfectly conducting, which implies that all MSM spheres that constitute a model are equipotential.

As shown in Fig. 1, MSM approximates a spacecraft as a collection of spheres with variable positions and radii. The voltage on any sphere is a function of both its

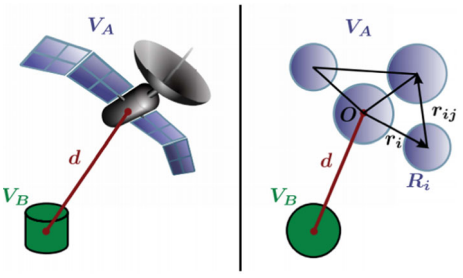

Fig. 1 Illustration of the MSM concept showing how two conducting space objects are decomposed into a series of body-fixed sphere with the same potential [20]

own charge and the charge of all nearby spheres. If these spheres are far enough away to be approximated as point charges, the voltage is given by: [19]

$$V_i = \frac{1}{4\pi\epsilon_0}\frac{q_i}{R_i} + \sum_{j=1,\, j\neq i}^{n} \frac{1}{4\pi\epsilon_0}\frac{q_j}{r_{i,j}} \tag{1}$$

where q_i and R_i are the charge and radius of the i^{th} sphere, respectively, $\rho_{i,\,j}$ is the center-to-center distance between spheres i and j, and ϵ_0 is the permittivity of free space constant. If the voltages of each sphere are given by $V = [V_1, V_2, ...V_n]^{\text{T}}$ and the charges are given by $q = [q_1, q_2, ...q_n]^{\text{T}}$, the relationship between the two is

$$V = [S]q \tag{2}$$

where $[S]$ is the elastance matrix defined below:

$$[S] = \frac{1}{4\pi\epsilon_0}\begin{bmatrix} 1/R_1 & 1/r_{1,2} & \cdots & 1/r_{1,n} \\ 1/r_{2,1} & 1/R_2 & \cdots & 1/r_{2,n} \\ \vdots & \vdots & \ddots & \vdots \\ 1/r_{n,1} & 1/r_{n,2} & \cdots & 1/R_n \end{bmatrix}\begin{bmatrix} q_1 \\ q_2 \\ \vdots \\ q_n \end{bmatrix} \tag{3}$$

If the voltage is known, the linear system can be solved for the charges q. For some simple systems, the charges can be found numerically [7], but for general models the charge is found numerically. Combining the charges with the locations of the spheres allows the force and torque to be computed.

The charge set $\mathbf{q}$ is calculated using Eq. 2. The charges, q_i, are used to calculate the electric field produced by the model, and forces and torques that an object model experiences subject to one or more external point charges. Denoting the position vector of an external point charge as $\mathbf{r}_k$ and the relative position vector of each MSM model sphere with respect to its center of mass as $\mathbf{r}_i$, the force, $\mathbf{F}$, and torque, $\mathbf{T}_{\text{O}}$, applied to the target model about its center of mass (O) by all external spheres with charges q_k are given in Eqs. 4 and 5 [20]

$$\mathbf{F} = -k_{\text{c}} \sum_{k=1}^{M} q_k \sum_{i=1}^{N} \frac{q_i}{||\mathbf{r}_{i,k}||^3}\mathbf{r}_{i,k} \tag{4}$$

$$\mathbf{T}_{\text{O}} = -k_{\text{c}} \sum_{k=1}^{M} q_k \sum_{i=1}^{N} \frac{q_i}{||\mathbf{r}_{i,k}||^3}\mathbf{r}_i \times \mathbf{r}_{i,k} \tag{5}$$

where $\mathbf{r}_{i,k}$ is the relative position of the k^{th} external sphere with respect to the i^{th} internal MSM sphere as shown in Fig. 1. Let N be the total number of spheres in the target model, while M is the total number of spheres external to the target such that $N_T = N + M$. Adding arbitrary numbers of external spheres does not add to the complexity of MSM modeling because they can be appended to the charge and elastance matrices; however, doing so will increase computational burden–primarily due growing size of the elastance matrix, which always needs to be inverted. Whole MSM models can be appended when the calculation of force and torque between two complex geometries is desired. The electric field at any point exterior to the spheres

of a MSM model is given by the superposition of the electric fields of each sphere, as shown in

$$\mathbf{E} = k_c \sum_{i=1}^{N_T} \frac{q_i}{||\mathbf{r}_{i,l}||^3} \mathbf{r}_{i,l} \tag{6}$$

where l is a point of interest in the space outside of the MSM model spheres, and $\mathbf{r}_{i,l}$ is the relative position between the i-th MSM model sphere and l.

Prior VMSM model fitting methods minimize a cost function based upon the difference between the force and torque vectors predicted by a VMSM model and the force and torque vectors generated by commercial FEM software. One such cost function is given in Reference [7] by

$$J = \frac{100}{2L} \left(\sum_{l=1}^{L} \frac{||\mathbf{F}_{\text{VMSM},l} - \mathbf{F}_{\text{FEM},l}||}{||\mathbf{F}_{\text{FEM},l}||} + \frac{||\mathbf{T}_{\text{VMSM},l} - \mathbf{T}_{\text{FEM},l}||}{||\mathbf{T}_{\text{FEM},l}||} \right) \tag{7}$$

where l has the same meaning as in Eq. 6 and L represents the total number of force and torque sample points. To alleviate far-field data noise effects in the optimization process, current methods utilize a self-capacitance constraint is proposed in Reference [7]. Enforcing the VMSM model match the self-capacitance of the target object ensures that the forces will match as the two objects get very far from each other. The self-capacitance C of a MSM model is given by [7]

$$C = \frac{Q}{V} = \frac{\sum_{i=1}^{N} q_i}{V} = \frac{1}{k_c} \sum_{i=1}^{N} \sum_{j=1}^{N} (S^{-1})_{ij} \tag{8}$$

where V is the scalar voltage of the conductor. To enforce a self-capacitance constraint, the self-capacitance of the target geometry is calculated using FEM and the MSM model self-capacitance is matched to the FEM result– reducing the optimizer search space by one dimension. The capacitance matching can be accomplished analytically for simple models, or numerically for large models. Matlab's *fmincon* optimizer allows the self-capacitance constraint to be defined in a constraint function and enforced numerically.

Electric Field VMSM Model Fitting

SMSM *E*-field Data Generation

Using the current VMSM methodology, the sphere positions and radii are varied by an optimizer to best match force and torque data produced by a commercial FEM program [7, 19, 20]. This methodology requires significant hand-tuning of model parameters for a model that fits force and torque data accurately due to noisy FEM data in the far field, dependance on probe size, and convergence properties of the force and torque cost function. Recent work largely streamlines the process of generating VMSM models using ANSYS Maxwell 3D to generate numerical data [7]. The workflow for current VMSM model fitting starts with generating solid models for a target and probe geometry in FEM software and calculating accurate force and

torque values between them at many relative positions. Self-capacitance of the target spacecraft is also calculated.

Generating the FEM truth data is by far the most time-consuming step. A complete sweep of locations for force and torque matching and validation may take hours and variations in accuracy depend heavily upon how many data points are used. In addition, complicated workarounds that automatically change probe radius are required to get accurate results when the object/probe separation distance is large. Current techniques use a spherical probe which has a radius that is a function of its distance from a target. The dependence on external probe geometry for force and torque calculations is clear in the above force and torque equations. This dependence is included into VMSM model generation when a cost function based on force and torque is used.

The workflow proposed in this paper seeks to address both of these issues. The initial step in modeling is the same — a single solid model of the target spacecraft is created. However, a solid model of external probe geometry is optional, and only used to gather limited force and torque data for verification of a model. A target voltage is prescribed and FEM software is used to calculate the self-capacitance of the target.

A SMSM model of the target geometry is then generated using any appropriate method. Note that the VMSM setup process in this paper is not tied to using SMSM in this step, but other fast methods such as a boundary element method or the method of moments could be used as well. All these solutions provide fast and accurate E-field predictions about a general shape. The SMSM method is used here because it provides a very smooth E-field prediction and it's simplicity to setup. One SMSM development method, appropriate for spherical and cylindrical geometries, is to use a golden spiral algorithm to distribute SMSM spheres on the surface of the geometry [20]. A method appropriate for flat geometries is to use a function like MATLAB's *meshgrid* to generate a distribution of sphere positions on the surface of a plane. This distribution can then be translated, rotated and combined with other planar distributions of spheres to form complex SMSM geometries [25]. When combining distributions, care should be taken to eliminate redundant spheres so that none overlap. Root finders like Matlab's *fsolve* can then be used with Eq. 8 to determine appropriate sphere radii to match the SMSM model self-capacitance to the self-capacitance of the solid model. Using the prescribed target voltage and Eq. 2, the charge on each SMSM sphere is calculated. Using the same equation applied to an N-sphere VMSM model optimization problem, an optimizer is used to select the optimal positions and radii of the model spheres to minimize the following cost function at sample points l

$$J\left(R_1, R_2, \ldots, R_N, \mathbf{r}_1, \mathbf{r}_2, \ldots, \mathbf{r}_N\right) = \sum_{l=1}^{L} \frac{||\mathbf{E}_{VMSM,l} - \mathbf{E}_{SMSM,l}||}{||\mathbf{E}_{SMSM,l}||} \tag{9}$$

where L is the total number of electric field sample points.

Using this cost function results in several major improvements to the prior methodology. The first improvement is the separation of VMSM model generations from any external probe geometry. Next, while the torques go to zero about particular symmetry axes, causing issues computing the relative MSM fit error, the E-field is always non-zero at any location relative to a charged spacecraft outside the convex hull

formed by its conducting surface. The final improvement is in the time required to complete all the steps in generating a VMSM model. Although the proposed E-field fitting methodology adds the step of creating a SMSM model for a given target geometry and voltage, this process requires significantly less computational effort than computing force at many relative positions with FEM. While the FEM takes a few minutes to compute the force and torque at each position, a SMSM model with a few hundred spheres will compute the electric field at a few tens or hundreds of positions in a less than a minute. Reference [7] discusses fitting to much smaller numbers of force and torque data points; however, using the proposed method, hundreds of data points are calculated rapidly and used to create a VMSM model in much less than the time it requires to calculate one force and torque calculation using commercial FEM software. A flowchart comparing the previous force and torque optimization procedure and the proposed E-field matching method is included in Fig. 2. The fitting speed are compared in detail in the following numerical simulation sections.

SMSM Validation

Before optimizing on a cost function built from a SMSM model, it is prudent to compare the accuracy of SMSM to other methods. The Method Of Images (MOI) provides an analytic infinite series solution to the problem of predicting the force between two spherical conductors [26, 27]. The method consists of placing smaller and smaller image charges within the body of each sphere to balance out the potential on the surfaces. As the number of image charges increases, the solution converges.

SMSM models of spheres are made with a variable number of spheres, and the force between the two bodies is compared to that predicted by MOI. For this case, two spheres with 1 meter radius are separated by 5 meters, and charged to ± 10 kV. The SMSM model is shown in Fig. 3a, an illustration for MOI showing the iterative charges is shown in Fig. 3b, and the results are plotted in Fig. 3c.

The x-axis indicates either the number of images charges used in each sphere for the MOI, or the number of individual spheres in each SMSM sphere. The MOI converges with 40 image charges, and SMSM converges with around 100 spheres. Since both methods converge to the same value, SMSM is validated as a method for predicting forces and torques on a sphere.

Now consider a more complex shape for which there is no analytical answer to compare to. In this case SMSM must be compared to an FEM program. Force and torque accuracy of a box-and-panel SMSM model with respect to FEM analysis is shown in Fig. 4. Average force and torque errors of the SMSM model are within a few percent of FEM-computed forces and torques.

The errors are shown via color in Fig. 4a and b and the shell-averaged error is shown in Fig. 4c. The color plots show that the error is concentrated across certain directions. For instance, the torque errors are greatest along the negative z axis. This is because the actual torque is very near zero along that direction and thus it is very susceptible to FEM grid noise. The shell-averaged errors also show some interesting structure - the errors initially drop from around 5% down to around 2.5% at near 10 meter separations, and then climb up to around 4% at 15 meters. This may be due to two opposite trends that become more or less dominant with distance. At very close

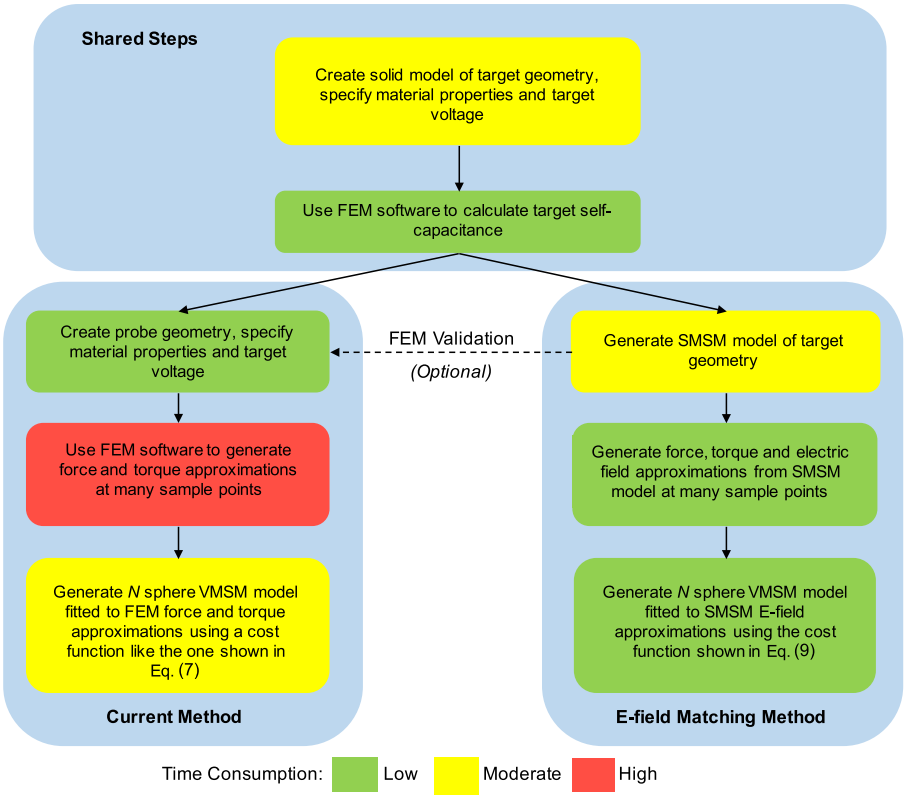

Fig. 2 Proposed workflow comparison with previous force and torque methods

distances ($\sim$ 5 meters), FEM performs very well and grid resolution is not a problem, but the relatively coarse nature of SMSM gives large errors. At medium distances ($\sim$10 meters) FEM is still performing well, but the increased distance causes grid resolution problems which increase FEM grid noise and decrease the accuracy of the FEM solution, however, SMSM increases in accuracy due to the increased separation distance. At far separations ($\sim$15 meters), the grid noise is very large which causes increased differences from the truth, even though SMSM is performing very well at this distance. It is thought that the middle region near 10 meters is where the increase in SMSM accuracy from being far apart best balance out the errors in FEM accuracy from grid noise.

Target Geometry, Data Generation and Optimization Methods

Two target geometries are used to compare the proposed E-field matching method to the previous force and torque method and to establish the accuracy of models generated using E-field matching. A two-sphere VMSM model is created for a charged

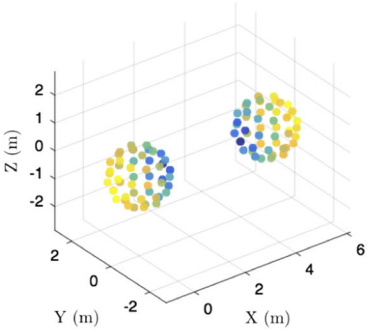

(a) SMSM schematic, color indicates charge

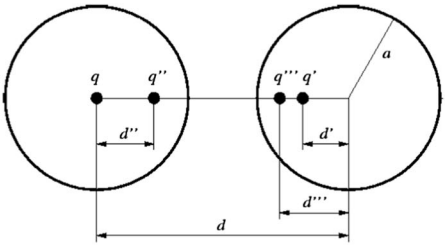

(b) MOI iterative image charge placement illustration

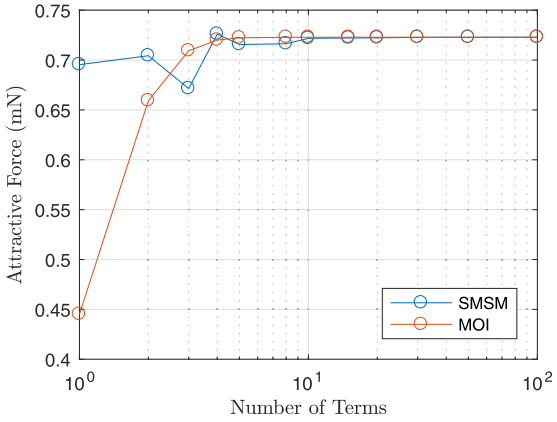

(c) Comparison Between MOI and SMSM

Fig. 3 Comparison of MOI and SMSM for predicting force on two spheres

cylinder, with a radius of 0.5 m and a height of 3 m, centered at the origin and oriented along the y-axis using the E-field matching method. This geometry is selected for easy comparison to previous work using force and torque matching [7, 19, 20].

Data for the study involving the cylinder geometry are generated at evenly spaced intervals on 90 degree arcs centered at the origin, lying in the x-y plane and in the fourth quadrant. The symmetry of the cylinder model requires data in only one quadrant for the optimization process. Force and torque data is generated using Maxwell 3D at the selected sample points. A SMSM model of the cylinder, shown in Fig. 5, is created to generate E-field data at the same sample points. Only sample points lying on the arc of a 5 m radius circle are used for optimization, as shown in Fig. 6a.

Two optimization methods are used to generate cylinder VMSM models: a global optimization method using Mathematica's Differential Evolution algorithm is used to optimize the force and torque cost function of Eq. 7, and MATLAB's *fmincon* local optimizer is used to minimize the E-field cost function of Eq. 9. Self-capacitance for

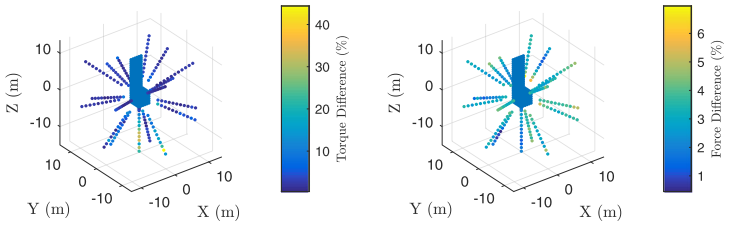

(a) SMSM Torque Error with Respect to FEM

(b) SMSM Force Error with Respect to FEM

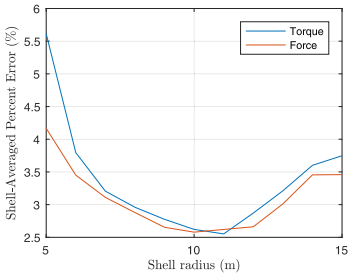

(c) SMSM Force and Torque Errors with Respect to FEM

Fig. 4 SMSM force and torque errors

the cylinder is calculated using Maxwell 3D. Both optimizers arrive at very nearly the same optimum despite them being global vs. local. This supports the idea that a local optimizer can find the global optimum with intuitive initial conditions.

Since a two-sphere VMSM model is used to represent the cylinder and the cylinder has symmetry about the x-axis, the VMSM model can be parameterized by one radius value r, which is shared by both spheres, and the separation distance, ρ, between the two spheres. This model is shown in Fig. 6b.

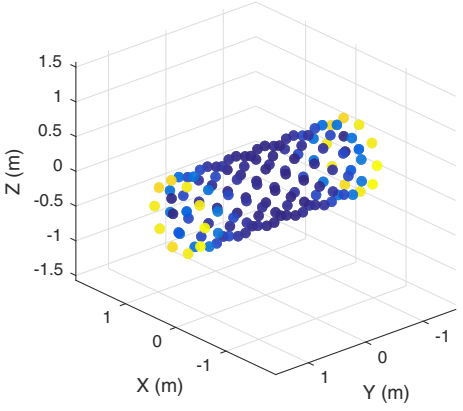

Fig. 5 SMSM model of a cylinder, color indicates charge

Using this model, an exact formula for the VMSM model self-capacitance can be derived [7]

$$C = \frac{1}{k_c} \frac{2r\rho}{r+\rho} \tag{10}$$

where r and ρ are the radius and separation of the spheres as shown in Fig. 6b. VMSM models that have the correct self-capacitance will correctly predict the total charge on the craft. In situations where the spacecraft can be modeled well as a point charge, such as debris towing in the far field, the force will also be correct. To match torques in the far field, the total charge and center of charge must be correct. In almost all cases, VMSM models that match self capacitance perform better than those that do not.

In addition, it reduces the optimization problem to one dimension, because for any r value there is only one corresponding ρ value for which the constraint is met. Solving (10) for ρ yields [7]

$$\rho = \frac{rC_{\text{mod}}}{2r - C_{\text{mod}}} \tag{11}$$

where

$$C_{\text{mod}} = k_c C \tag{12}$$

Since C_{mod} is a scaling of the self-capacitance, it is used to impose the self-capacitance constraint in the following studies because its value is on the order of model parameters. Both the optimal r and ρ values are solved for using *fmincon* and the self-capacitance constraint is imposed numerically.

The second target spacecraft geometry that is selected for this study is a box-and-panel satellite modeled as a cube shaped bus with a long, slender panel attached. The bus width, height and depth are 3 m. The panel width is 3 m, depth is 0.2 m and height is 8.5 m. The panel is located on the top of the bus extending in the z-axis direction with one of its large faces coplanar with the positive y face of the bus. This model

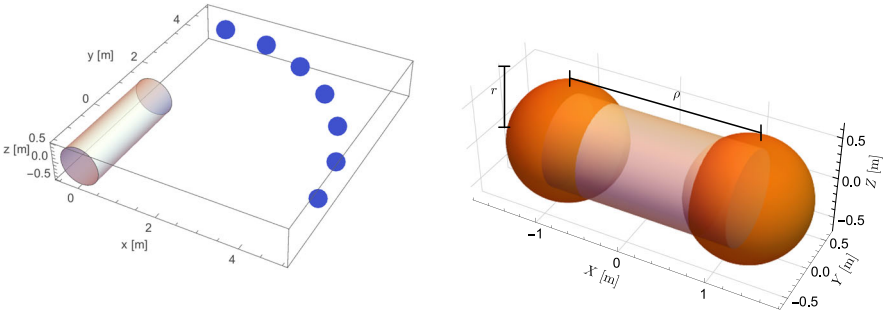

(a) Distribution of Sample Points Around Cylinder (b) Two-Sphere VMSM Cylinder Model with Parameter Annotations[7]

Fig. 6 Cylinder data distribution and VMSM model parameters

geometry is shown in Fig. 7. This geometry is selected because it has significant variation from simple geometric shapes like cylinders and represents a more realistic target spacecraft. It also shows symmetry that can be used to impose additional constraints on the positions of the VMSM model spheres, and this symmetry is exploited to reduce the amount of data that is required for the optimization procedure.

A SMSM model of the box-and-panel is generated using MATLAB's *meshgrid* feature to create many rectangles which are translated and rotated to make the full spacecraft, and electric field data is generated using Eq. 6, at positions spread radially about the SMSM model. Sample points are generated using the golden spiral algorithm, which places equally spaced points on the surface of a sphere [24]. This radial spread of electric field data produces distributions of shells of data, which are easily selected or neglected, or reduced to hemispheres or octants for fitting, such as the one shown in Fig. 7. Whole spherical shells of data are produced for the box-and-panel geometry; however, due to the symmetry of the model, the complete behavior of the electric field produced by the SMSM model can be captured in one hemisphere of data.

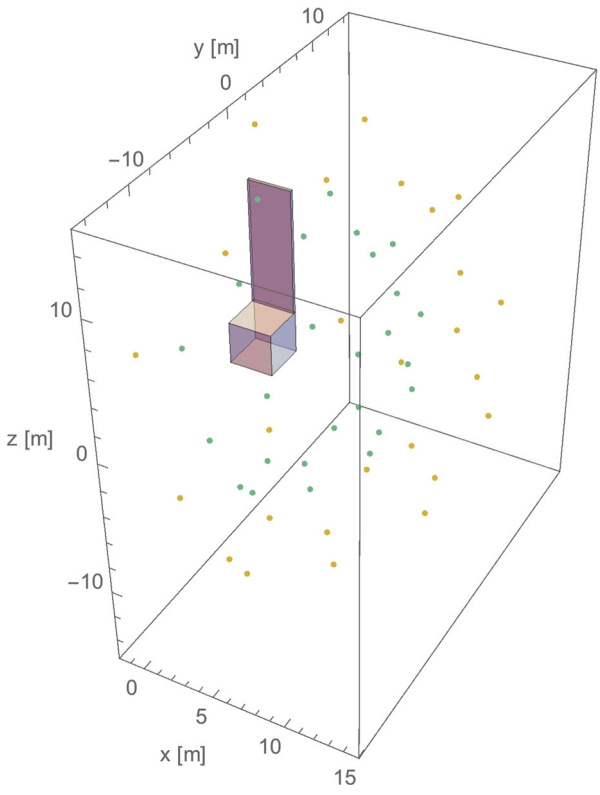

Fig. 7 Box-and-Panel Geometry with Data Point Distribution

One, two and three-sphere VMSM reduced-coordinate models are created with this data using E-field matching and MATLAB's *fmincon* optimization algorithm. Various sets of data, including whole spheres, hemispheres and multiple shell sets, are used in the optimization processes. In addition, a three-sphere 4 degree-of-freedom VMSM model is generated using E-field matching and *fmincon*. Only shells with radii larger than 12 m are used for optimization to avoid overlap between sample points and SMSM spheres, which would invalidate Eq. 6. Like the cylinder model optimization process, the box-and-panel self-capacitance is calculated using Maxwell 3D and the self-capacitance constraints on the optimization processes are imposed numerically. Additional inequality constraints are imposed for the two and three-sphere VMSM models to ensure aesthetically pleasing models in which spheres do not overlap.

Cost Function Comparison

The cost function of Eq. 7 is compared with the proposed electric field cost function of Eq. 9 to compare their characteristics. Both cost functions are used to generate two-sphere VMSM models for a perfectly conducting cylinder charged to 30 kV. Maxwell 3D is used to determine a cylinder self-capacitance value of 106.8345 pF. Noting a potential singularity in Eq. 11 when r is one half C_{mod}, the cost function values, shown in Fig. 8a and b, along the intersection with the self-capacitance constraint surface are plotted against r for which ρ is positive. The force and torque cost function is evaluated across one quadrant and shell of FEM-generated force and torque predictions. The E-field cost function is evaluated across the same quadrant and shell, but using SMSM-generated E-field predictions.

The r values minimizing both cost functions are nearly identical, differing by only 0.2%. Investigating the cost function sensitivities near both minima suggests that force and torque errors are more sensitive to model parameters than E-field errors are. The proposed E-field cost function shows desirable characteristics, particularly for a local optimization algorithm like *fmincon*. It is generally smooth when compared with the force and torque cost function, and apart from a small region near the singularity in ρ, approaches its minimum unimpeded.

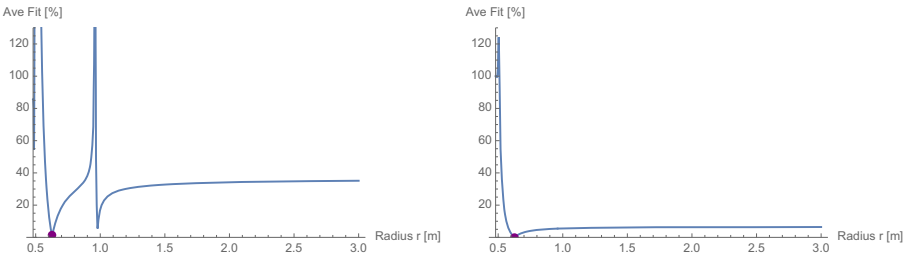

(a) Former Force and Torque Cost Function (b) New E-field Cost Function

Fig. 8 Force and torque and E-field cost functions for cylinder model

Constrained and Unconstrained Box-and-Panel VMSM Models

One, two and three-sphere box-and-panel VMSM models are generated with and without a self-capacitance constraint in order to determine the usefulness of the constraint when applied to an optimization problem without far-field data noise. Models are fit to data in three whole spherical shells with radii of 15, 20 and 25 m. Symmetry of the box-and-panel geometry about the $y-z$ plane is used to reduce the $4N$ degree-of-freedom optimization problem to a $3N$ degree-of-freedom problem. Imposing a self-capacitance constraint reduces the degrees-of-freedom to $3N-1$. The model is charged to 30 kV. Maxwell 3D is once again used to calculate self-capacitance, and returns a value of 336.14 pF. Optimizer initial conditions are chosen loosely based on the box-and-panel geometry. A visualization the VMSM models of the box-and-panel geometry is included in Fig. 9.

Tables 1, 2, and 3 show the initial and final conditions for the one, two, and three-sphere box-and-panel models, with and without the self-capacitance constraint.

Shell-averaged force and torque errors of the six VMSM models with respect to the SMSM generated data are shown in Fig. 10a and b, respectively. As can be seen, the self-capacitance constraint has utility even when far-field noise is not a concern. In particular, when generating a one-sphere model the self-capacitance constraint ensures that force errors far from the target geometry continue to decay as sample point radius is increased. The effect of the self-capacitance constraint is also dramatic for the two-sphere model. The force errors of the two and three-sphere models are nearly identical at 30 m from the target geometry when the constraint is imposed, whereas without it the two-sphere model model force errors remain significantly larger than the three-sphere model's. It is interesting to note that, as more spheres are added to the VMSM model, self-capacitance is matched automatically as displayed by the three-sphere force and torque errors. Both the constrained and non-constrained model errors overlap, and the optimal model parameters of each are nearly identical.

Another benefit of imposing the self-capacitance constraint is that it can significantly reduce computational effort. The number of function calls required to generate each of the six models is recorded. The results are shown in Fig. 11. The results show that imposing the self-capacitance constraint consistently results in increased performance regardless of how many spheres are used to create the VMSM model. This performance increase is due to the reduced dimension of the search space when a self-capacitance constraint is enforced. Given the increased force and torque accuracy and decreased computation effort, the self-capacitance constraint should be enforced even when far-field noise is not a concern.

Reduced-Shell Data Sets with Self-Capacitance Constraint

Since imposing a self-capacitance constraint forces force vectors in the far-field to automatically match, it is desired to investigate whether or not fewer numbers of shells with smaller radii can be used to effectively generate VMSM models. This question is interesting for two reasons: smaller data sets will reduce the amount of

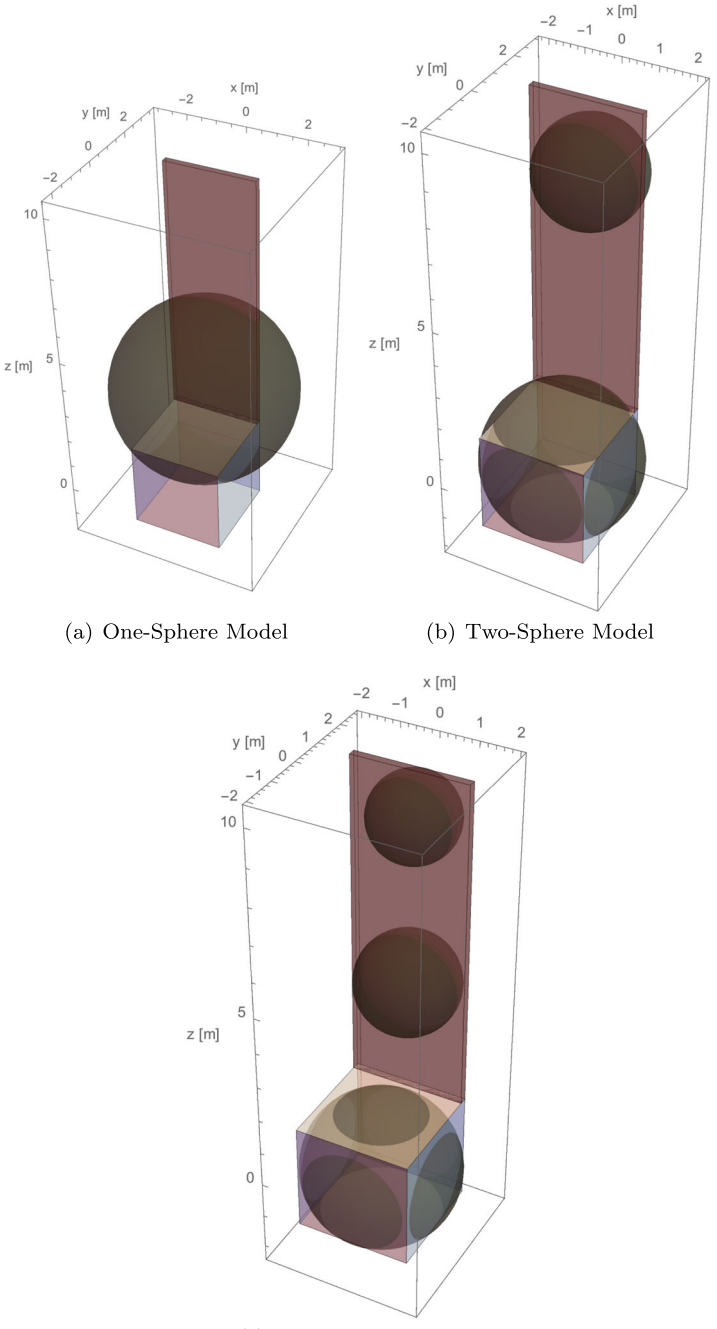

(a) One-Sphere Model

(b) Two-Sphere Model

(c) Three-Sphere Model

Fig. 9 Visualizations of VMSM box-and-panel geometry models generated using the E-field fitting method

Table 1 Initial and final states for one-sphere VMSM model optimization, C- Constrained, NC- Non-Constrained

	R_1 [m]	y_1 [m]	z_1 [m]
Initial	1.000	0.000	0.000
Final C	3.021	0.626	2.914
Final NC	2.951	0.608	2.785

time required for optimization, and fitting to data closer to the target might increase near-field accuracy without significantly affecting accuracy at larger distances.

A three-sphere VMSM model is used to model the box-and-panel geometry. The VMSM model is fit to single shells at radii of 12, 14 and 15 m. The model voltage is set to 30 kV, and a self-capacitance constraint of 336.14 pF is imposed. The accuracy of these models are compared with each other and to the three-sphere constrained model generated using three whole shells. The resulting shell-averaged force, torque, and average error plots when compared with the SMSM model are shown in Fig. 12a, b, and c.

These results show negligible differences in force and torque accuracy near the target, while the model fitted to the 12 m radius shell shows degraded accuracy far from the target. Accuracies of models fit to three whole shells and to 14 m and 15 m shell radii are nearly identical. The practical impact of the degraded accuracy for the model fitted to the 12 m shell is very small; however, for high accuracy at large distances from a target, a model should be fitted to at least one shell with a larger radius.

The performance impact of reducing the number of shells is analyzed by recording the number of *fmincon* iterations and total time required to generate each model. The results are shown in Fig. 13a and b. These results show that there is not necessarily a positive correlation between decreased numbers of data points and increased performance. Fitting to data points very close to the target geometry increases the number of iterations required to generate a model. In addition, the time required to generate a model is not solely dependent upon the number of data points. While it takes more time to generate a model using three whole shells of data when compared to one whole shell at a radius of 15 m, it takes approximately the same amount of time to generate a model using one whole shell with a radius of 12 m even though the number of *fmincon* iterations is 12% less. The competing interests of maintaining a self-capacitance constraint while fitting to electric field data near the target – which

Table 2 Initial and final states for two-sphere VMSM model optimization, C- Constrained, NC- Non-Constrained

	R_1 [m]	R_2 [m]	y_1 [m]	z_1 [m]	y_2 [m]	z_2 [m]
Initial	1.000	1.000	0.000	0.000	1.400	6.000
Final C	2.202	1.458	0.135	0.210	1.596	8.183
Final NC	2.201	1.471	0.134	0.207	1.600	8.177

Table 3 Initial and Final States for Three-Sphere VMSM Model Optimization, C- Constrained, NC- Non-Constrained

	R_1 [m]	R_2 [m]	R_3 [m]	y_1 [m]	z_1 [m]	y_2 [m]	z_2 [m]	y_3 [m]	z_3 [m]
Initial	1.000	1.000	1.000	0.000	0.000	1.400	6.000	1.400	9.000
Final C	2.039	1.323	1.120	− 0.008	− 0.166	1.319	4.584	1.555	8.972
Final NC	2.041	1.322	1.119	− 0.007	− 0.163	1.321	4.612	1.556	8.974

is far more variable than the same data at larger radii – is likely the reason for this phenomenon. Due to the increased error and decreased performance associated with fitting to shells very close to the target, it is recommended to fit models using shells at intermediate ranges. Doing so aids convergence of the optimizer, and the total time required to generate a model is decreased either because the number of iterations to convergence is decreased or because the total time required for one iteration of the optimizer is decreased, or both.

Modeling using General 4 Degree-of-Freedom MSM Spheres

Previous work focuses on simple geometries that have high levels of symmetry, like the cylinder model. For geometries like these, the number of MSM optimization parameters can be reduced significantly by specifying, for example, that the cylinder MSM spheres must lie on the symmetry axis. As geometric complexity increases, so does the effort required to find symmetries to exploit and analytically parameterize them. Using general MSM 4 degree-of-freedom (4DOF) modeling allows each MSM sphere to have 3 location and one radius degree of freedom. This avoids the need to find symmetry and allows for optimization in a $4N$ dimension search space. Each parameter associated with a VMSM model sphere is found through optimization, and the up-front human-involvement cost of generating a model is reduced.

A three-sphere VMSM model of the box-and-panel geometry is generated using data in three whole shells with radii of 15, 20 and 25 m. A self-capacitance constraint

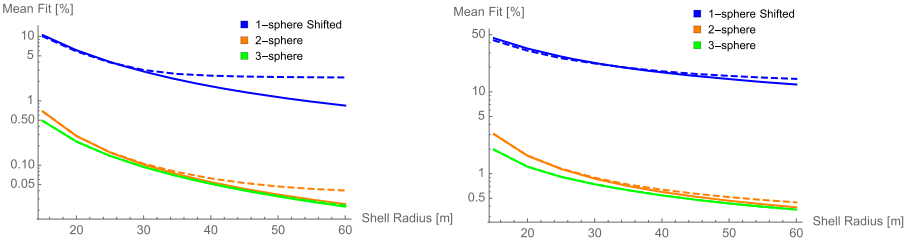

(a) Force Errors (b) Torque Errors

Fig. 10 One, two and three sphere VMSM model force and torque errors with respect to SMSM force and torque predictions, (—) constrained, (- -) non-constrained

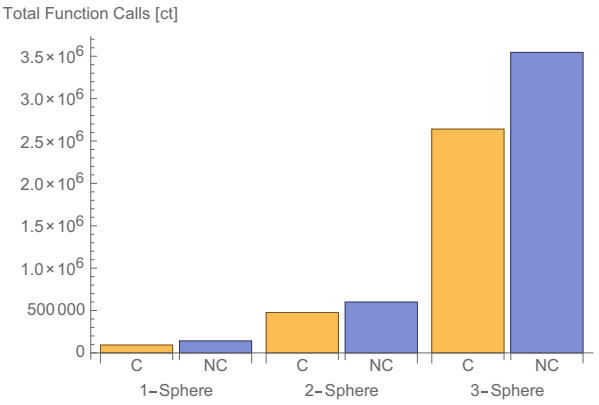

Fig. 11 Total matlab function calls required to generate one, two and three-sphere box-and-panel VMSM models using E-field fitting

is enforced using a value of 336.14 pF. The model voltage is set to 30 kV. The initial and final conditions for the 4DOF fitting problem are shown in Table 4.

The force and torque accuracy of the 4DOF model with respect to the box-and-panel SMSM model is compared to three-sphere 3DOF models using three whole shells and one half shell at 15 m in Fig. 14a and b.

The model with the least accuracy is the 3DOF model fitted to one half shell of data. The 4DOF model's accuracy resembles the 3DOF model fitted to three whole shells. Since the optimizer knows nothing about the symmetry of the box-and-panel

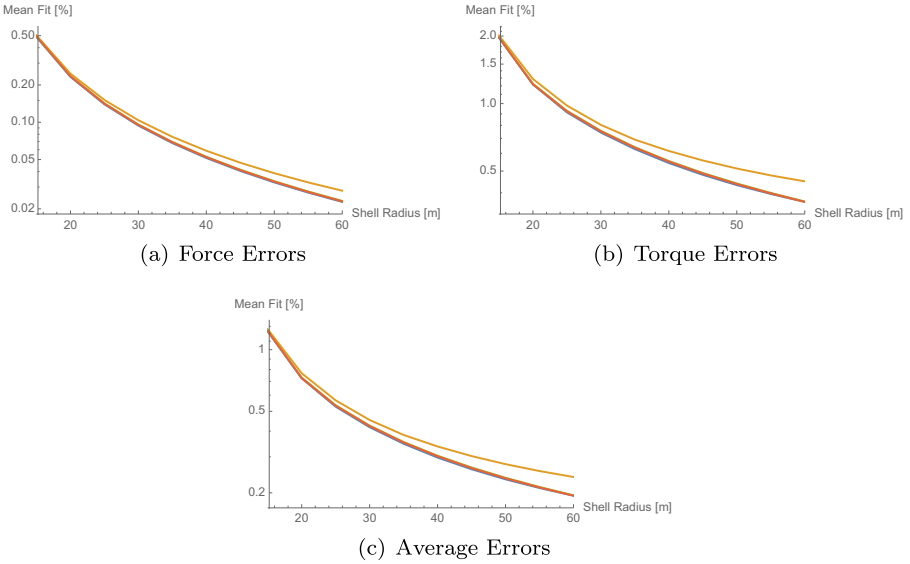

Fig. 12 Model force, torque and average (force and torque) errors of three-sphere box-and-panel VMSM models generated using: (—) 3 Whole Shells, (—) 15 m Shell, (—) 14 m Shell, (—) 12 m Shell

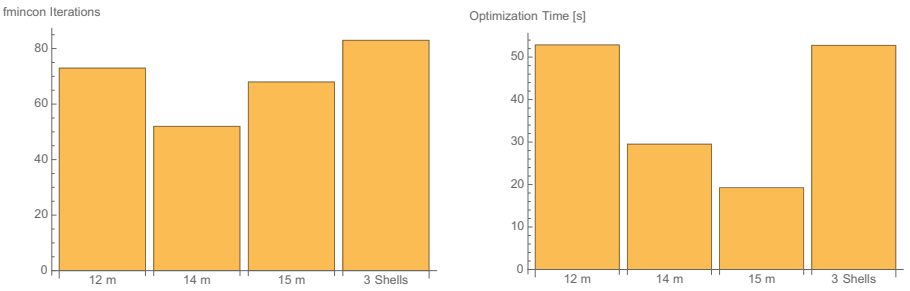

(a) *fmincon* Iterations (b) Total Model Generation Times

Fig. 13 *fmincon* iterations and total model generation times required to generate three sphere VMSM models using E-field fitting and shell reduction for various SMSM-generated E-field data sets

model, a whole shell of data must be used to generate an accurate model when 4DOF is used. Total *fmincon* iterations for each of the models shown in Fig. 14 are shown in Table 5.

Surprisingly, the 4DOF modeling method yields a converged result using only 58% of the iterations required for a 3DOF model using a half shell of data with the same radius. These results reiterate that the number of iterations required for convergence upon a useful model is far more dependent on using data at intermediate radii than on the number of data points used. However, when considering time required to generate a model, the 3DOF 1 half shell model is by far the most efficient to generate, requiring only about a third as much time as the three whole shell models. An interesting result is that the 4DOF model is generated in approximately the same amount of time as the 3DOF 3 whole shell model. These results show that 4DOF modeling using E-field fitting is promising from both an accuracy and performance perspective, and a 4DOF can be generated in approximately the same amount of time as a 3DOF model using the same number of data points at the same shell radii.

Table 4 Initial and Final States for Three-Sphere 4DOF VMSM Model Optimization

	Initial	Final
R_1 [m]	1.000	2.051
R_2 [m]	1.000	1.299
R_3 [m]	1.000	1.106
x_1 [m]	0.000	− 0.004
y_1 [m]	0.000	− 0.004
z_1 [m]	0.000	− 0.136
x_2 [m]	0.000	0.038
y_2 [m]	1.400	1.385
z_2 [m]	6.000	4.788
x_3 [m]	0.000	− 0.028
y_3 [m]	1.400	1.534
z_3 [m]	9.000	8.993

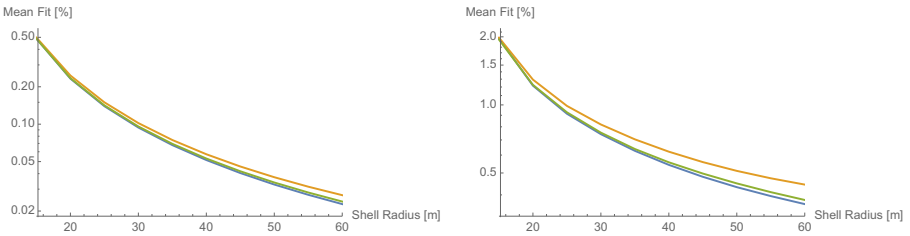

(a) Force Errors (b) Torque Errors

Fig. 14 4DOF force and torque percent relative error comparison to SMSM force and torque predictions for: (—) three-sphere model three whole shells, (—) three-sphere model one half shell, (—) three-sphere model one whole shell (4DOF)

Future Work

The performance of the E-field matching method suggests that the results of the cost function analysis can be extrapolated to higher dimension search spaces; however, more research into the convergence properties of the E-field fitting technique should be carried out. Although a self-capacitance constraint is imposed in this work, other appropriate constraints might be found to further reduce the dimension of the search space and aid performance. Research into the convergence properties of the E-field matching method might lead the way to fully autonomous model generation using 4DOF VMSM models.

Moreover, in this paper local optimization algorithms are used extensively with no guarantee that the resulting VMSM models are globally optimal in any sense. The results show that, in many cases, practical accuracy requirements can be met in a very short time using local optimization algorithms. Experience shows that local optimization using intuitive initial conditions and reasonable bounds on the search space lead to practically identical sphere radii and placement as global optimization; however, the new E-field cost function is similarly disadvantaged as previous force and torque cost functions in that it is not convex. Given time reductions in generating models when using local optimization are profound in their own right, research in optimality guarantees using this method can be very valuable. Although it is not expected that other cost functions used in the literature to-date or different optimization algorithms applied to the same geometry will yield significantly different results from the ones shown in this paper, closer investigation into the impact of different cost functions and optimization algorithms might yield interesting results.

Table 5 Total function calls for 4DOF model comparison

Model	Total *fmincon* Iterations
4DOF 3 Whole Shells	77
3DOF 3 Whole Shells	83
3DOF 1 Half Shell	132
3DOF 1 Whole Shell	68

The selected target geometry represents a particular target of interest that might be found at GEO. The box-and-panel target geometry is not representative of all objects of interest, and VMSM modeling of more complicated geometries should be investigated. These geometries should be selected to represent a healthy cross section of potential targets at GEO. An assumption is made in this work that the target is a perfect conductor, but many objects of interest have dielectric properties. Extension of this work to model dielectrics is a worthwhile pursuit.

Conclusion

This paper introduces a new way to create a VMSM model using electric field matching rather than force and torque matching. This new method has four main benefits: first, finite element grid noise is no longer an issue in the far field; second, probe geometry is no longer tied to the solution; third, the solution is much faster to produce; and lastly the cost function is much smoother and easier to optimize. Using E-field matching and VMSM sphere populations provides highly accurate fits with respect to SMSM models with lower computational burden than previously explored methods. The presented E-field matching fits to smooth, analytically generated data, does not rely on probe geometry and has a simpler cost function that easily leverages self-capacitance constraints to increase computational efficiency, improve force and torque fits far from a target and reduce the amount of data required for optimization. The improvements with E-field matching over previously studied methods is apparent in the more rapid convergence of two and three-sphere VMSM models of a box-and-panel spacecraft. The proposed E-field matching method provides a more suitable approach for complicated spacecraft geometries and higher degree-of-freedom optimizations due to reduced computational time and improved fit accuracy. E-field matching provides a fast and simple means of generating VMSM models for electrostatic modeling of fully conducting space objects.

Acknowledgment This research is funded through a grant No. FA9550-15-1-0407 from the Air Force Office of Space Research.

References

1. Früh, C., Ferguson, D., Lin, C., Jah, M.: The effect of passive electrostatic charging on Near-Geosynchronous high Area-To-Mass ratio objects. Int. Astron. Congr. **64**, 2094–2103 (2013)
2. Hughes, J., Schaub, H.: Rapid charged geosynchronous debris perturbation modeling of electrodynamic disturbances. J. Astronaut. Sci. **65**(2), 135–156 (2018)
3. Peck, M.A.: Prospects and Challenges for Lorentz-Augmented Orbits. In: AIAA Guidance, Navigation and Control Conference, San Francisco, CA (2005). Paper No. AIAA 2005-5995
4. Cover, J.H., Knauer, W., Maurer, H.A.: Lightweight reflecting structures utilizing electrostatic inflation. US Patent 3,546,706 (1966)
5. King, L.B., Parker, G.G., Deshmukh, S., Chong, J.-H.: Spacecraft Formation-Flying using Inter-Vehicle Coulomb Forces, tech. rep., NASA/NIAC. http://www.niac.usra.edu (2002)
6. Schaub H., Moorer, D.F.: Geosynchronous large debris reorbiter: challenges and prospects. J. Astronaut. Sci. **59**(1–2), 161–176 (2014). https://doi.org/10.1007/s40295-013-0011-8

7. Chow, P., Hughes, J., Bennett, T., Schaub, H.: Automated Sphere Geometry Optimization for the Volume Multi-sphere Method, AAS/AIAA Space Flight Mechanics Meeting, No. AAS-16-672, Napa Valley, California (2016)
8. Paul, S.N., Frueh, C.: Space debris charging and its effect on orbit evolution. american institute of aeronautics and astronautics (2016)
9. Schaub H., Sternovsky, Z.: Active space debris charging for contactless electrostatic disposal maneuvers. In: 6th European Conference on Space Debris, Darmstadt, Germany, ESOC (2013). Paper No. 6b.O-5
10. Bennett, T., Stevenson, D., Hogan, E., McManus, L., Schaub, H.: Prospects And challenges of touchless debris despinning using electrostatics. Adv. Space Res. **56**, 557–568 (2015). https://doi.org/10.1016/j.asr.2015.03.037
11. Peck, M.A., Streetman, B., Saaj, C.M., Lappas, V.: Spacecraft formation flying using lorentz forces. J. Br. Interplanet. Soc. **60**, 263–267 (2007)
12. Sobiesiak, L.A., Damaren, C.J.: Lorentz-Augmented Spacecraft formation reconfiguration. In: AIAA/AAS Astrodynamics Specialist Conference, San Diego, California (2014)
13. Streetman, B., Peck, M.A.: General bang-bang control method for lorentz augmented orbits. J. Spacecr. Rocket. **47**, 484–492 (2010). https://doi.org/10.2514/1.45704
14. Hogan, E.A., Schaub, H.: General high-altitude orbit corrections using electrostatic tugging with charge control. J. Guid. Control. Dyn. **28**, 699–705 (2015). https://doi.org/10.2514/1.G000092
15. Hogan, E., Schaub, H.: Relative motion control for Two-Spacecraft electrostatic orbit corrections. AIAA J. Guid. Control. Dyn. **36**, 240–249 (2013)
16. Bennett, T., Schaub, H.: Touchless electrostatic detumbling while tugging large axi-symmetric GEO Debris. In: AAS/AIAA Space Flight Mechanics Meeting, Williamsburg, VA (2015). Paper AAS 15-383
17. Bennett, T., Schaub, H.: Touchless Electrostatic Three-Dimensional detumbling of large Axi-Symmetric debris, Journal of astronautical sciences (2015)
18. Schaub, H., Bennett, T., Hughes, J.: Current developments in three-dimensional electrostatic detumble of axi-symmetric GEO Debris. In: 4th International Workshop on Space Debris Modeling and Remediation, CNES, Paris (2016). Paper No. 6.4
19. Stevenson, D., Schaub, H.: Multi-Sphere Method for modeling electrostatic forces and torques. Adv. Space Res. **51**, 10–20 (2013). https://doi.org/10.1016/j.asr.2012.08.014
20. Stevenson, D.: Optimization of sphere population for electrostatic multi sphere model. In: 12th Spacecraft Charging Technology Conference, Kitakyushu, Japan (2012)
21. Smythe, W.R.: Static and Dynamic Electricity. McGraw–Hill 3rd ed. (1968)
22. Gibson, W.C.: The method of moments in electromagnetics. Chapman & hall (2007)
23. Lai, S.T.: Fundamentals of spacecraft charging: Spacecraft interactions with space plasmas. Princeton University Press (2011)
24. Bauer, R.: Distribution of points on a sphere with application to star catalogs. J. Guid. Control. Dyn. **23**(1), 130–137 (2000)
25. Schaub, H.: Faster-than-realtime Electrostatic Force and Torque Modeling for SSA Applications. AFOSR Annual Report, University of Colorado, Aerospace Engineering Sciences Department, Boulder, CO (2016)
26. Maxwell, J.: A treatise on electricity and magnetism. Oxford University Press (1893)
27. Lekner, J.: Electrostatics of two charged conducting spheres. Proc. R. Soc. **468**, 2829–2848 (2012)